

Higher multipole and retardation corrections to the dipole angular distributions of *L*-shell photoelectrons ejected by polarized photons

A. Bechler* and R. H. Pratt

Department of Physics and Astronomy, University of Pittsburgh, Pittsburgh, Pennsylvania 15260

(Received 9 April 1990)

We calculate first-retardation and multipole corrections to the dipole angular distributions of *L*-shell photoelectrons ejected by polarized photons. The calculation is performed nonrelativistically in the framework of the independent-particle model. It leads to general expressions for the *s* and *p* subshell retardation correction in terms of radial matrix elements and relative phase shifts. In the *2s* case the retardation effects may contribute as much as 10–30% to the angular distribution even close to threshold, especially for higher-*Z* elements. In the *2p* case the retardation effects are small close to threshold but can contribute as much as 10–20% for relatively low final electron energies of 1–3 keV. We have also obtained simple semianalytical expressions for the retardation corrections, based on the assumption that for inner shells screening effects beyond normalizations and phase shifts can be treated perturbatively. The semianalytic formulas compare quite well with the results of numerical calculations for the *2s* subshell; they are somewhat worse for *2p* photoelectrons, especially for lower energies and lower *Z*. This is due to the fact that in the latter case larger distances become more important in the integrals determining radial matrix elements. In the *2s* case the retardation effects result in forward or backward peaking of the angular distributions. For the *2p* initial state and linearly polarized photons, they lead to deviations from dipole predictions for a uniform angular distribution of photoelectrons whose momenta are perpendicular to the direction of photon polarization.

I. INTRODUCTION

The purpose of this paper is to present results of a calculation of first-retardation corrections to the dipole angular distribution of the photoelectrons ejected from the *L* shell by polarized photons. The calculation is performed in the framework of the independent-particle model. In a previous paper¹ we gave results of a similar calculation (with unpolarized photons) for *K*-shell photoelectrons. As in that paper, we mean by the first-retardation corrections a contribution to the photoeffect amplitude corresponding to a term linear in $\mathbf{k}\cdot\mathbf{r}$ in the expansion of the photon plane wave. This term gives a large photon wavelength ($k\rightarrow 0$) limit of the electric quadrupole contributions to the amplitude, whereas the nonrelativistic dipole approximation [replacing $\exp(i\mathbf{k}\cdot\mathbf{r})$ by unity] gives the large-wavelength limit of the electric dipole.

In the dipole approximation the angular distribution of photoelectrons ejected by linearly polarized photons depends on the angle between the polarization direction and the direction of the outgoing electron momentum, and is described by the well-known formula²

$$\frac{d\sigma}{d\Omega} = \frac{\sigma}{4\pi} [1 + \beta P_2(\cos\theta)], \quad (1)$$

where β is the asymmetry parameter, θ is the angle between the photon polarization vector and electron momentum, and σ represents the total cross section. In general, however, the angular distribution of photoelec-

trons ejected by linearly polarized photons depends on two angles: the angle θ between the photon polarization vector and the electron momentum (which may be chosen as the polar angle in the coordinate system in which the photon polarization is along the *z* direction) and the azimuthal angle Φ . More generally, the polarized angular distribution depends on two scalar products, $\mathbf{p}\cdot\mathbf{k}$, $\mathbf{p}\cdot\boldsymbol{\epsilon}$, where \mathbf{p} , \mathbf{k} , and $\boldsymbol{\epsilon}$ denote the electron momentum, photon momentum, and the photon polarization vector, respectively. In the dipole approximation, only the dependence on $\mathbf{p}\cdot\boldsymbol{\epsilon}$ remains.

Dependence of the angular distribution of photoelectrons ejected by polarized photons on both angles can be seen in a theoretical cross section only if one goes beyond the dipole approximation. This means, in the first approximation, either including next-to-dipole (i.e., electric quadrupole) terms in the full multipole expansion of the amplitude, or, at low photoelectron energy when the large-wavelength limit is justified, expanding the photon plane wave up to and including terms linear in $\mathbf{k}\cdot\mathbf{r}$. (The multipole expansion corresponds to an angular-momentum decomposition of the amplitudes, so that electron wave functions have been expanded in partial waves, the vector potential of the photon in vector spherical harmonics.) This last expansion, which we call the retardation expansion, mixes various multipoles in terms corresponding to given powers of $\mathbf{k}\cdot\mathbf{r}$ and should not be confused with the multipole expansion.¹ It is only the large-wavelength ($k\rightarrow 0$) limit of the multipole series that corresponds to the retardation expansion.

General relativistic formulas for the photoelectron an-

gular distribution with polarized photons and electrons including the complete multipole expansion of the photon field have been given previously.^{3,4} In the present paper we perform a nonrelativistic calculation using the nonrelativistic expressions for the transition matrix element together with the nonrelativistic bound and continuum electron wave functions, not taking into account the electron spin. Including terms $\sim \mathbf{k} \cdot \mathbf{r}$ results in a retardation correction proportional to v/c , where v is the continuum electron velocity.^{1,5} The relativistic correction to the nonrelativistic matrix element is $\sim (v/c)^2$ or $(Z\alpha)^2$, so that it is expected to be small (at low energies) compared to the first-retardation contribution. We do not attempt to use the general formulas given in Refs. 3 and 4 in the nonrelativistic limit. In general, one does not expect that the nonrelativistic ($c \rightarrow \infty$) limit of these general expressions gives the same results as the *ab initio* nonrelativistic calculation. This is due mainly to the presence of the electron spin, which does not decouple when $c \rightarrow \infty$. That is, the initial electron bound state is, also in the limit, the eigenstate of the total angular momentum \mathbf{J} (which is the good quantum number in the relativistic approach), rather than the eigenstate of orbital angular momentum and spin separately, as is usual in the nonrelativistic approach. Also, in the $c \rightarrow \infty$ limit we expect the presence of the Pauli-Schrödinger term in the matrix element,⁶ which couples the electron spin to the photon wave magnetic field and which is of order k ; this term is not taken into account in the fully nonrelativistic calculation.⁷

In the next section, we derive nonrelativistic expressions for the photoeffect matrix elements when the initial electron is in the p subshell. By calculating the modulus squared and summing over the initial magnetic quantum number, but not over photon polarization, we obtain angular distributions with polarized photons. At the beginning of this section, we also quote the formula describing the angular distribution when the initial electron is in the s state. They have basically the same form as those given in Ref. 1. In Sec. III we discuss results of the numerical calculation of the parameters describing the $2s$ and $2p$ photoelectron angular distribution in the case of linearly polarized photons. We note here the differences between the $1s$ and $2s$ cases, as well as some similarities between $1s$ and $2p$ cases. The differences in the shapes of retardation corrections for $1s$ and $2s$ initial state are due to the $2s$ bound wave function having a node, whereas the $1s$ bound-state function is always positive. The similarities between the $1s$ and $2p$ cases can be related to the fact that both $1s$ and $2p$ bound-state wave functions have no node. We see in general that the retardation corrections in the energy range considered here (threshold to a few keV) are a little smaller in the $2p$ case than in the $1s$ case, especially for higher values of Z . This can be contrasted with the relatively large values of the retardation correction in the $2s$ case. In Sec. III we also perform a comparison of the numerical results with the semianalytic approach of the same type as that described in Ref. 1. Section IV contains final remarks, and some details of the calculations from Sec. II have been put into the Appendix.

We use natural units $\hbar = m = c = 1$, where m is the electron mass.

II. FORMULAS FOR THE RETARDATION CORRECTION TO THE ANGULAR DISTRIBUTION OF L -SHELL PHOTOELECTRONS

A general expression for the bound-free transition matrix element in the independent-particle approximation reads

$$M_{fi} = \langle f | e^{i\mathbf{k} \cdot \mathbf{r}} \boldsymbol{\epsilon} \cdot \mathbf{P} | i \rangle, \quad (2)$$

where f and i denote the final and initial electron state, respectively, \mathbf{k} is the photon momentum and $\boldsymbol{\epsilon}$ is its polarization vector, and \mathbf{P} is the momentum operator. To calculate the amplitude up to and including the first-retardation correction, we expand the photon plane wave up to and including terms linear in \mathbf{k} . The resulting angular distribution formula with unpolarized photons for the $1s$ initial electron state has been given previously.¹ The general structure of the angular distribution of the s -subshell photoelectrons is the same, so that we can write, after formula (10) in Ref. 1,

$$M_{fi}^{(ns)} = 4\pi i (\boldsymbol{\epsilon} \cdot \mathbf{p}) (\alpha_1 e^{i\delta_1} + \alpha_2 e^{i\delta_2} k \hat{\mathbf{p}} \cdot \hat{\mathbf{k}}), \quad (3)$$

where the index ns denotes the subshell of the initial electron, and $\hat{\mathbf{p}}, \hat{\mathbf{k}}$ denote unit vectors in the directions of \mathbf{p} and \mathbf{k} , respectively (\mathbf{p} is the momentum of final electrons). The radial matrix elements α_l are given by

$$\alpha_l = \int_0^\infty dr r^{l+1} R_l \frac{dR_{ns}}{dr}, \quad (4)$$

where R_l, R_{ns} are the radial wave functions of the final and initial electron, respectively. Expression (4) for radial matrix elements corresponds to the velocity form of the transition matrix element. In a similar way as in the standard dipole approximation (or large-wavelength limit of the "true" electric-dipole amplitude), one can pass to the length form; details of this type of a calculation in the case when the quadrupole contribution is taken into account will be shown below for the p initial subshell.

The angular distribution of the ns photoelectrons ejected by polarized photons is given by

$$\frac{d\sigma^{(ns)}}{d\Omega} = A |\boldsymbol{\epsilon} \cdot \hat{\mathbf{p}}|^2 (1 + \kappa \hat{\mathbf{p}} \cdot \hat{\mathbf{k}}), \quad (5)$$

where the retardation correction κ to the dipole $|\hat{\mathbf{e}} \cdot \hat{\mathbf{p}}|^2$ -type angular distribution can be written as

$$\kappa = k \frac{Q_2}{D_1} \cos(\delta_2 - \delta_1), \quad (6)$$

with the length form of the quadrupole (Q_2) and dipole (D_1) matrix element in the large-wavelength limit given by⁸

$$D_1 = \int_0^\infty dr r^2 R_1 r R_{n0}, \quad Q_2 = \int_0^\infty dr r^2 R_2 r^2 R_{n0}. \quad (7)$$

It is evident from (5) that when the initial electron is in the s subshell, the photon polarization effects appear only as an overall factor in the angular distribution. In the coordinate system in which the z axis is along the photon polarization vector and the photon momentum is along the x axis [Fig. 1(a)], formula (5) can be written as

$$\frac{d\sigma^{(ns)}}{d\Omega} = A \cos^2\theta(1 + \kappa \sin\theta \cos\Phi), \quad (8)$$

with the angles θ and Φ the same as in Fig. 1(a). Directing now the photon momentum along \mathbf{k} and the x axis along $\boldsymbol{\epsilon}$, we get [Fig. 1(b)]

$$\frac{d\sigma^{(ns)}}{d\Omega} = A \sin^2\theta_1 \cos^2\Phi_1 (1 + \kappa \cos\theta_1). \quad (9)$$

For the unpolarized angular distribution, we obtain

$$\frac{d\sigma_{\text{unpol}}^{(ns)}}{d\Omega} = A \sin^2\theta_1 (1 + \kappa \cos\theta_1), \quad (10)$$

with θ_1 being the angle between \mathbf{p} and \mathbf{k} .

We now calculate the transition matrix element (1) with the first-retardation correction for the p -subshell initial electron state. This can be done either by expanding the final electron wave function and photon plane wave in a partial wave series, and then picking up terms of a given order in k from the photon partial waves (as has been done in Ref. 1), or by expanding the plane wave right at the beginning:

$$\exp(i\mathbf{k}\cdot\mathbf{r}) \approx 1 + i\mathbf{k}\cdot\mathbf{r}. \quad (11)$$

In the present calculation, we use (11) rather than the previous method, mainly because it allows for a simpler transition to the length form of the matrix element.

Subsequent calculation will be done without specifying any particular coordinate system. The final formulas for the angular distribution will then be written in two coordinate systems depicted in Fig. 1. We write Eq. (2) using the expansion (11),

$$M_{fi} = \langle f | (1 + i\mathbf{k}\cdot\mathbf{r})(\boldsymbol{\epsilon}\cdot\mathbf{P}) | i \rangle. \quad (12)$$

The large-wavelength limit of the dipole contribution can be written in the length form

$$M_{fi}^{\text{dipole}} = -\omega \langle f | \boldsymbol{\epsilon}\cdot\mathbf{r} | i \rangle, \quad (13)$$

where $\omega = E_f - E_i$ is the photon energy and E_f (E_i) is the final (initial) electron energy. To transform the retardation correction into the length form, we use

$$[H, \mathbf{r}] = -i\mathbf{P}, \quad (14)$$

where H is the one-electron Hamiltonian

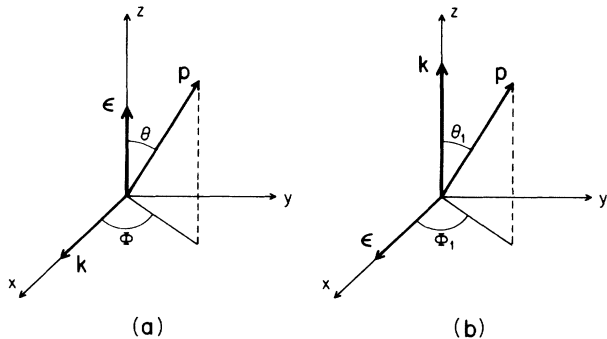


FIG. 1. The coordinate systems used in the discussion of the photoelectron angular distribution.

$$H = \frac{\mathbf{P}^2}{2} + V(r), \quad (15)$$

with the self-consistent potential $V(r)$. The retardation correction can now be written as

$$\begin{aligned} M_{fi}^{\text{ret}} &\equiv i \langle f | (\mathbf{k}\cdot\mathbf{r})(\boldsymbol{\epsilon}\cdot\mathbf{P}) | i \rangle \\ &= E_i \langle f | (\mathbf{k}\cdot\mathbf{r})(\boldsymbol{\epsilon}\cdot\mathbf{r}) | i \rangle - \langle f | (\mathbf{k}\cdot\mathbf{r})H(\boldsymbol{\epsilon}\cdot\mathbf{r}) | i \rangle. \end{aligned} \quad (16)$$

This can be further transformed into

$$\begin{aligned} M_{fi}^{\text{ret}} &= -\omega \langle f | (\mathbf{k}\cdot\mathbf{r})(\boldsymbol{\epsilon}\cdot\mathbf{r}) | i \rangle - \langle f | [\mathbf{k}\cdot\mathbf{r}, H](\boldsymbol{\epsilon}\cdot\mathbf{r}) | i \rangle \\ &= -\omega \langle f | (\mathbf{k}\cdot\mathbf{r})(\boldsymbol{\epsilon}\cdot\mathbf{r}) | i \rangle - i \langle f | (\mathbf{k}\cdot\mathbf{P})(\boldsymbol{\epsilon}\cdot\mathbf{r}) | i \rangle. \end{aligned} \quad (17)$$

Using

$$(\mathbf{k}\cdot\mathbf{P})(\boldsymbol{\epsilon}\cdot\mathbf{r}) = (\boldsymbol{\epsilon}\cdot\mathbf{P})(\mathbf{k}\cdot\mathbf{r}) + (\boldsymbol{\epsilon}\times\mathbf{k})\cdot(\mathbf{r}\times\mathbf{P}), \quad (18)$$

we get

$$\begin{aligned} M_{fi}^{\text{ret}} &\equiv i \langle f | (\mathbf{k}\cdot\mathbf{r})(\boldsymbol{\epsilon}\cdot\mathbf{P}) | i \rangle \\ &= -\omega \langle f | (\mathbf{k}\cdot\mathbf{r})(\boldsymbol{\epsilon}\cdot\mathbf{r}) | i \rangle - i \langle f | (\mathbf{k}\cdot\mathbf{r})(\boldsymbol{\epsilon}\cdot\mathbf{P}) | i \rangle \\ &\quad - i \langle f | (\boldsymbol{\epsilon}\times\mathbf{k})\cdot(\mathbf{r}\times\mathbf{P}) | i \rangle, \end{aligned} \quad (19)$$

and finally

$$M_{fi}^{\text{ret}} = -\frac{1}{2}\omega k \langle f | (\hat{\mathbf{k}}\cdot\mathbf{r})(\boldsymbol{\epsilon}\cdot\mathbf{r}) | i \rangle - \frac{i}{2}(\boldsymbol{\epsilon}\times\mathbf{k})\cdot\langle f | \mathbf{L} | i \rangle, \quad (20)$$

where \mathbf{L} is the orbital-angular-momentum operator. The first term in Eq. (20) gives the large-wavelength limit of the electric quadrupole contribution, and the second one corresponds to the magnetic dipole. Due to orthogonality, the magnetic-dipole term gives a vanishing contribution, so that for the transition matrix element with first-retardation correction we get

$$M_{fi} = -\omega \langle f | \boldsymbol{\epsilon}\cdot\mathbf{r} | i \rangle - \frac{1}{2}k\omega \langle f | (\hat{\mathbf{k}}\cdot\mathbf{r})(\boldsymbol{\epsilon}\cdot\mathbf{r}) | i \rangle. \quad (21)$$

The wave function of the electron in the initial bound state has the form

$$\psi_i = R_{np}(r)Y_{1m}(\hat{\mathbf{r}}) \quad (22)$$

and the continuum electron wave function will be expanded in a partial wave series

$$\psi_f = \sum_{l=0}^{\infty} i^l (2l+1) e^{-i\delta_l} P_l(\hat{\mathbf{p}}\cdot\hat{\mathbf{r}}) R_l(r), \quad (23)$$

with obvious notation. The dipole rules pick up terms with $l=0$ and $l=2$ in ψ_f , whereas the quadrupole contribution is a sum of $l=1$ and $l=3$ terms (generally of $l-2$, l , and $l+2$ terms, but in the present case $l-2 < 0$). Explicitly, we have

$$\begin{aligned} \langle f | \boldsymbol{\epsilon}\cdot\mathbf{r} | i \rangle &= \frac{4\pi}{3} \{ e^{i\delta_0} D_0 Y_{1m}(\boldsymbol{\epsilon}) \\ &\quad + e^{i\delta_2} D_2 [Y_{1m}(\boldsymbol{\epsilon}) - 3(\boldsymbol{\epsilon}\cdot\hat{\mathbf{p}})Y_{1m}(\hat{\mathbf{p}})] \}, \end{aligned} \quad (24)$$

where $Y_{lm}(\hat{\mathbf{n}})$ denotes the spherical harmonic whose arguments are the polar and azimuthal angles of the unit

vector $\hat{\mathbf{n}}$, and D_0, D_2 are the usual dipole matrix elements appearing, in the large-wavelength limit, in the dipole contribution to the transition matrix element

$$D_l = \int_0^\infty dr r^2 R_l(r) R_{np}(r). \quad (25)$$

$$\begin{aligned} \langle f | (\hat{\mathbf{k}} \cdot \mathbf{r})(\boldsymbol{\epsilon} \cdot \mathbf{r}) | i \rangle = & -\frac{4\pi}{5} i e^{i\delta_1} Q_1 [(\boldsymbol{\epsilon} \cdot \hat{\mathbf{p}}) Y_{1m}(\hat{\mathbf{k}}) + (\hat{\mathbf{p}} \cdot \hat{\mathbf{k}}) Y_{1m}(\boldsymbol{\epsilon})] \\ & + \frac{4\pi}{5} i e^{i\delta_3} Q_3 [-(\boldsymbol{\epsilon} \cdot \hat{\mathbf{p}}) Y_{1m}(\hat{\mathbf{k}}) - (\hat{\mathbf{p}} \cdot \hat{\mathbf{k}}) Y_{1m}(\boldsymbol{\epsilon}) + 5(\boldsymbol{\epsilon} \cdot \hat{\mathbf{p}})(\hat{\mathbf{p}} \cdot \hat{\mathbf{k}}) Y_{1m}(\hat{\mathbf{p}})], \end{aligned} \quad (26)$$

where Q_1 and Q_3 are the quadrupole radial matrix elements in the large-wavelength limit

$$Q_l = \int_0^\infty dr r^2 R_l(r) r^2 R_{np}(r). \quad (27)$$

The shape of the photoelectron angular distribution up to and including the first-retardation correction is given by

$$\frac{d\sigma^{(np)}}{d\Omega} \sim \sum_m [|M^{\text{dipole}}|^2 + 2 \operatorname{Re}(M^{\text{dipole}} M^{*\text{ret}})]. \quad (28)$$

Substituting (24) and (26) and using the summation formula for spherical harmonics,

$$P_l(\hat{\mathbf{a}} \cdot \hat{\mathbf{b}}) = \frac{4\pi}{2l+1} \sum_{m=-l}^l Y_{lm}^*(\hat{\mathbf{a}}) Y_{lm}(\hat{\mathbf{b}}), \quad (29)$$

we obtain

$$\begin{aligned} \sum_m |M_{fi}|^2 = & \frac{4\pi}{3} \omega^2 \{ D_0^2 + 2D_2^2 + (2D_2^2 - 4D_0 D_2 \cos\Delta_{20}) P_2(|\boldsymbol{\epsilon} \cdot \hat{\mathbf{p}}|) \\ & + \frac{3}{5} k [(\hat{\mathbf{p}} \cdot \hat{\mathbf{k}}) F_{01} + (\hat{\mathbf{p}} \cdot \hat{\mathbf{k}})(1 - 5|\boldsymbol{\epsilon} \cdot \hat{\mathbf{p}}|^2) F_{03} + (\hat{\mathbf{p}} \cdot \hat{\mathbf{k}})(1 - 6|\boldsymbol{\epsilon} \cdot \hat{\mathbf{p}}|^2) F_{21} + (\hat{\mathbf{p}} \cdot \hat{\mathbf{k}})(1 + 4|\boldsymbol{\epsilon} \cdot \hat{\mathbf{p}}|^2) F_{23}] \}, \end{aligned} \quad (30)$$

where

$$\Delta_{ll'} = \delta_l - \delta_{l'}, \quad F_{ll'} = D_l Q_{l'} \cos\Delta_{ll'}. \quad (31)$$

The dipole combination has been cast into the familiar form with the second Legendre polynomial and the asymmetry parameter, which from (30) can be seen to be

$$\beta = \frac{2D_2^2 - 4D_0 D_2 \cos\Delta_{20}}{D_0^2 + 2D_2^2}, \quad (32)$$

as expected. Since the first-retardation correction is either quadratic or of zero order in $|\boldsymbol{\epsilon} \cdot \hat{\mathbf{p}}|$, it can be also expressed in terms of $P_2(|\boldsymbol{\epsilon} \cdot \hat{\mathbf{p}}|)$. Simple calculation gives

$$\frac{d\sigma}{d\Omega} = \frac{\sigma}{4\pi} \{ 1 + \beta P_2(|\boldsymbol{\epsilon} \cdot \hat{\mathbf{p}}|) + (\hat{\mathbf{p}} \cdot \hat{\mathbf{k}}) [a + b P_2(|\boldsymbol{\epsilon} \cdot \hat{\mathbf{p}}|)] \}, \quad (33)$$

where σ is the total cross section, and

$$a = k \frac{\frac{3}{5} F_{01} - \frac{3}{5} F_{21} - \frac{2}{5} F_{03} + \frac{2}{5} F_{23}}{D_0^2 + 2D_2^2}, \quad (34a)$$

$$b = k \frac{\frac{8}{5} F_{23} - 2F_{03} - \frac{12}{5} F_{21}}{D_0^2 + 2D_2^2}, \quad (34b)$$

with $F_{ll'}$ given by (31). Summing over photon polarizations, we find

Details of the calculation leading to (24) as well as to the electric quadrupole term [(26) below] are given in the Appendix. The dipole term (24) leads of course to the well-known dipole angular distribution (1). For the electric quadrupole term, we obtain

$$\begin{aligned} \left. \frac{d\sigma}{d\Omega} \right|_{\text{unpol}} = & \frac{\sigma}{4\pi} [1 + B_1 P_1(\hat{\mathbf{p}} \cdot \hat{\mathbf{k}}) \\ & + B_2 P_2(\hat{\mathbf{p}} \cdot \hat{\mathbf{k}}) + B_3 P_3(\hat{\mathbf{p}} \cdot \hat{\mathbf{k}})], \end{aligned} \quad (35)$$

where

$$B_1 = a - \frac{1}{5} b = \frac{3}{10} k \frac{\frac{18}{5} F_{23} - \frac{2}{5} F_{21} + 2F_{01}}{D_0^2 + 2D_2^2}, \quad (36a)$$

$$B_2 = -\frac{1}{2} \beta = -\frac{D_2^2 - 2D_0 D_2 \cos\Delta_{20}}{D_0^2 + 2D_2^2}, \quad (36b)$$

$$B_3 = -\frac{3}{10} b = \frac{3}{10} k \frac{2F_{03} - \frac{8}{5} F_{23} + \frac{12}{5} F_{21}}{D_0^2 + 2D_2^2}. \quad (36c)$$

Expressions (36) for B_n coefficients agree with the formulas obtained previously by Wang⁹ for the unpolarized angular distribution with the first-retardation correction.

Choosing a coordinate system with the z axis along the linear polarization vector and the x axis along the photon momentum [Fig. 1(a)], we obtain

$$\frac{d\sigma}{d\Omega} = \frac{\sigma}{4\pi} \{ 1 + \beta P_2(\cos\theta) + \sin\theta \cos\Phi [a + b P_2(\cos\theta)] \}. \quad (37)$$

In the coordinate system in which the z axis is along the photon momentum and the x axis is along the polarization vector [Fig. 1(b)], we have

$$\frac{d\sigma}{d\Omega} = \frac{\sigma}{4\pi} \left\{ 1 + \frac{1}{2}\beta(3\sin^2\theta_1\cos^2\Phi_1 - 1) + \cos\theta_1 \left[a + \frac{1}{2}b(3\sin^2\theta_1\cos^2\Phi_1 - 1) \right] \right\}. \quad (38)$$

Using

$$\begin{aligned} \sin^2\theta_1 &= \frac{2}{3}[1 - P_2(\cos\theta_1)], \\ \cos\theta_1\sin^2\theta_1 &= \frac{2}{3}[P_1(\cos\theta_1) - P_3(\cos\theta_1)], \\ \cos^2\Phi_1 &= \frac{1}{2}(\cos 2\Phi_1 + 1), \end{aligned} \quad (39)$$

Eq. (38) can be written as

$$\begin{aligned} \frac{d\sigma}{d\Omega} = \frac{\sigma}{4\pi} \{ & 1 + B_1P_1(\cos\theta_1) + B_2P_2(\cos\theta_1) + B_3P_3(\cos\theta_1) \\ & - \cos^2\Phi_1[6^{1/2}B_2d_{20}^2(\theta_1) \\ & + (\frac{10}{3})^{1/2}B_3d_{20}^3(\theta_1)] \}, \end{aligned} \quad (40)$$

where

$$\begin{aligned} d_{20}^2(\theta_1) &= \frac{3}{2}6^{-1/2}\sin^2\theta_1, \\ d_{20}^3(\theta_1) &= \frac{5}{2}(\frac{3}{10})^{1/2}\cos\theta_1\sin^2\theta_1, \end{aligned} \quad (41)$$

are the (2,0) matrix elements of the rotation matrices in the $l=2$ and 3 representations of the rotation group. Equation (40) is a particular form of the general formula obtained by Huang.⁴

Formula (33) can also be written for the case of an arbitrary photon polarization (complete or partial). Using the Stokes parameters¹⁰ ξ_1, ξ_2, ξ_3 , we need to make the replacement

$$|\epsilon \cdot \hat{\mathbf{p}}|^2 \rightarrow \frac{1}{2}\sin^2\theta_1(1 + \xi_1\cos 2\Phi_1 + \xi_2\sin 2\Phi_1),$$

where the angles θ_1 and Φ_1 are shown in Fig. 1(b). For the angular distribution, we obtain

$$\begin{aligned} \frac{d\sigma}{d\Omega} = \frac{\sigma}{4\pi} \{ & 1 + B_1P_1(\cos\theta_1) + B_2P_2(\cos\theta_1) + B_3P_3(\cos\theta_1) \\ & - (\xi_1\cos 2\Phi_1 + \xi_2\sin 2\Phi_1) \\ & \times [6^{1/2}B_2d_{20}^2(\theta_1) + (\frac{10}{3})^{1/2}B_3d_{20}^3(\theta_1)] \}. \end{aligned} \quad (42)$$

We can see that in the nonrelativistic approximation the angular distribution of photoelectrons ejected by polarized photons is determined by the same three parameters that determined angular distribution in the unpolarized case, i.e., B_1, B_2, B_3 or, equivalently, β, a , and b [cf. (33)]. The general relativistic expression for the photoelectron angular distribution in the case of polarized incident photons reads⁴

$$\begin{aligned} \frac{d\sigma}{d\Omega} = \frac{\sigma}{4\pi} \left[& 1 + \sum_{l \geq 1} B_{0l}P_l(\cos\theta_1) \right. \\ & \left. - (\xi_1\cos 2\Phi_1 + \xi_2\sin 2\Phi_1) \sum_{l \geq 2} B_{1l}d_{20}^l(\theta_1) \right], \end{aligned} \quad (43)$$

with, in principle, independent sets of parameters B_{0l} and

B_{1l} [B_{0l} corresponds to B_l in (42)]. In the nonrelativistic approximation to the p -subshell photoelectron angular distribution, we found that there are simple relations between some of these parameters, namely

$$B_{12} = 6^{1/2}B_{02}, \quad B_{13} = (\frac{10}{3})^{1/2}B_{03}, \quad (44)$$

and there are only three independent parameters, not five. The first of the relations (44), corresponding to the dipole angular distribution, has also been given in Ref. 4. One may expect that, in the nonrelativistic approach, the angular distribution with polarized photons will be described by the same number of independent parameters as in the unpolarized case up to an arbitrary order in the retardation expansion, though we do not have a general proof. One should also expect more relations of the type (44).

III. NUMERICAL RESULTS AND DISCUSSION

In this section, we discuss results of the numerical calculation of the retardation correction to the dipole angular distributions of $2s$ and $2p$ photoelectrons. We also give simple semianalytic formulas for these corrections, which agree quite well with the numerical calculation. The numerical calculations were performed with the use of the program PHOTO.¹¹

A. The $2s$ case

The $2s$ angular distribution is described by formula (5):

$$\frac{d\sigma(2s)}{d\Omega} = A|\epsilon \cdot \hat{\mathbf{p}}|^2(1 + \kappa \cos\theta), \quad (45)$$

where

$$\kappa = k \frac{Q_2}{D_1} \cos(\delta_2 - \delta_1), \quad (46)$$

where the dipole and quadrupole matrix elements in the large-wavelength approximation, D_1 and Q_2 , respectively, are given by (7). In Fig. 2 we show the $2s$ retardation correction κ as a function of the photoelectron energy. A comparison with the $1s$ case,¹ displayed in Fig. 3, shows that both the general shapes of the curves and the signs of κ at threshold for various values of Z are now different. The extrema of $\kappa(2s)$ are in general more pronounced than in the $1s$ case, and for larger Z the retardation correction has both a maximum and a minimum in the energy range considered here, whereas the $1s$ retardation correction only had a minimum. Among the cases shown in Fig. 2, the maximum is especially visible for $Z=36$. For all three cases shown in Fig. 2 ($Z=6, 10$ and 36), the sign of $\kappa(2s)$ at threshold is opposite to that for $1s$ photoelectrons. In Table I we show the values of $\kappa(2s)$ at threshold, with $\kappa(1s)$ also shown for comparison.

It was noted previously¹ that the sign of the $1s$ retardation correction coincides with the sign of $\cos(\delta_2 - \delta_1)$. In this case, both Q_2 and D_1 are positive from threshold to high energies. This changes in the present $2s$ case with $Q_2 < 0$ and $D_1 > 0$ at low energies and Q_2 changing sign once. Therefore, the sign of $\kappa(2s)$ at threshold is opposite

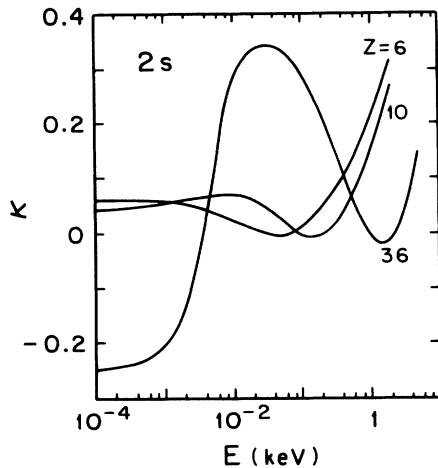


FIG. 2. Retardation correction κ [Eq. (46)] to the angular distribution of 2s photoelectrons as a function of energy.

to that of $\cos(\delta_2 - \delta_1)$, and, at the same time, opposite to the sign of $\kappa(1s)$ for the same value of Z .

The negative sign of $Q_2(2s)$ at low energy can be explained by noting that, contrary to the 1s bound-state wave function, the 2s wave function for $Z=10$ has a node at a distance of $\approx 0.1 \text{ \AA}$ from the nucleus and for $Z=36$ at $\approx 0.03 \text{ \AA}$, and is negative for distances bigger than that at which the node occurs. With the continuum radial function positive for $r=0$ and starting to oscillate (at low energies) for rather large distances, at which the bound-state wave function is already small, a significant portion of the integration comes from the region where the integrand is negative. In the present case, this region dominates for Q_2 but not for D_1 . Compared to the dipole matrix element, the quadrupole matrix element at small distances has two more powers of r in the integrand, which diminishes the contribution from the region where the integrand is positive, leading to negative values of Q_2 . Though the integrand of D_1 also vanishes at the origin, due to the smaller power of r (for $r \rightarrow 0$) the region where the integrand is positive contributes more than in the Q_2

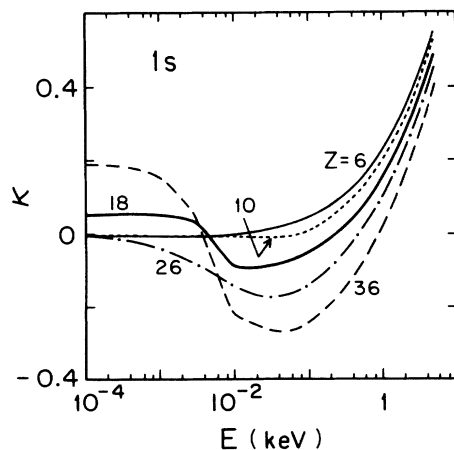


FIG. 3. Retardation correction to the angular distribution of 1s photoelectrons (Ref. 1). These results are shown here for the purpose of comparison with the 2s and 2p cases.

TABLE I. First retardation correction to the 2s photoelectron angular distribution at threshold. 1s retardation (Ref. 1) is shown for comparison.

Z	$\kappa(2s)$	$\kappa(1s)$
6	5.92×10^{-2}	-5.77×10^{-3}
8	4.96×10^{-2}	-4.19×10^{-3}
10	3.96×10^{-2}	-2.92×10^{-3}
12	6.73×10^{-3}	-1.30×10^{-3}
14	-4.14×10^{-2}	1.21×10^{-2}
16	-9.23×10^{-2}	3.37×10^{-2}
18	-1.21×10^{-1}	5.08×10^{-2}
20	5.15×10^{-2}	-2.60×10^{-2}
22	3.12×10^{-2}	-1.72×10^{-2}
24	5.60×10^{-2}	-3.24×10^{-2}
26	2.02×10^{-3}	-1.24×10^{-2}
28	-8.45×10^{-3}	5.39×10^{-3}
30	-1.67×10^{-2}	1.10×10^{-2}
32	-1.15×10^{-1}	7.98×10^{-2}
34	-1.87×10^{-1}	1.36×10^{-1}
36	-2.49×10^{-1}	1.89×10^{-1}
38	5.68×10^{-2}	-4.54×10^{-2}
40	4.30×10^{-2}	-3.58×10^{-2}

case, so that D_1 is positive. With increasing energy of the final electron, the oscillations of the continuum wave function damp the contribution from larger distances, moving the dominant region of integration toward the origin, so that the quadrupole matrix element Q_2 becomes positive with increasing energy. The position of the zero of Q_2 increases with Z , which is connected to the fact that the node of the bound-state wave function moves toward the origin with increasing Z and, to obtain a positive integral, the continuum wave function must start oscillating at smaller distance, which means higher energy.

This discussion is somewhat related to a recent discussion of whether the number of zeros in the radial matrix elements is even or odd.¹² The general theory described in that paper predicts an odd number of zeros in the quadrupole radial matrix element (in the long-wavelength limit) for the transition from a bound ns state ($n > 1$) to an ed final continuum state (cf. Table I in Ref. 11). This agrees with the presence of one zero in our Q_2 quadrupole radial matrix element. The theory also predicts an odd number of zeros (i.e., at least one zero) in the dipole matrix element for the transitions from the ns ($n > 1$) state to the ep state. The zero in some cases can occur in the negative energy regime. Manson¹³ has pointed out that for 2s no zero occurs in the continuum. This agrees with our result, where we observe no zero in the dipole D_1 radial matrix element for positive electron energies.¹⁴ We also note that a reasoning of the type presented in the previous paragraph does not apply to the quadrupole $l \rightarrow l-2$ and $l \rightarrow l$ transitions (which do not occur for s subshells). According to Ref. 12, the radial matrix elements in these two cases have an even number of zeros, so that, in particular, there may be no zero in Q_l or Q_{l-2} . The reason we cannot apply our previous argument to the $l \rightarrow l, l-2$ transitions is that for lower angular momenta the continuum radial function starts to oscillate

sooner and may damp the contribution from regions where the integrand is negative.

Due to the zero of Q_2 , the $2s$ retardation correction has one more zero than $\cos(\delta_2 - \delta_1)$, i.e., one more zero than $\kappa(1s)$ for the same value of Z . For instance, in the $Z=6$ case (Fig. 2), there is a zero of $\kappa(2s)$ at $E \approx 0.03$ keV, corresponding to a zero of $\cos(\delta_2 - \delta_1)$, and a zero at $E \approx 0.07$ keV connected with a zero of Q_2 . A minimum of the curve occurs between these two energies and, since the positions of the two zeros are close to each other and neither $\cos(\delta_2 - \delta_1)$ nor Q_2/D_1 vary rapidly, the value of $\kappa(2s)$ at minimum is small. A similar pattern can be seen for $Z=10$ with a zero of $\cos(\delta_2 - \delta_1)$ at $E \approx 0.08$ keV and a zero of Q_2 at $E \approx 0.2$ keV. The $2s$ retardation correction for $Z=36$ has three zeros, with the first two of them being due to the zeros of $\cos(\delta_2 - \delta_1)$ and the last one coming from Q_2 . Again, the position of the second zero at $\cos(\delta_2 - \delta_1)$ and of the zero of Q_2 are close to each other, so that the value of $\kappa(2s)$ at its minimum is small.

We also performed a comparison of the numerical results for $\kappa(2s)$ with the approximate semianalytic expression, analogous to that considered in Ref. 1. In the semianalytic approach we write the ratio Q_2/D_1 as

$$\frac{Q_2}{D_1} = \frac{N_2}{N_1} \frac{Q_2'}{D_1'} \quad (47)$$

where N_l are the normalization factors of corresponding continuum radial functions, and Q_2' and D_1' are approximated by corresponding point-Coulomb expressions, with the shifted energy E_c determined by the point-Coulomb energy conservation equation

$$E_c = \omega - \frac{1}{8}(Z\alpha)^2 \quad (48)$$

This approximation, which is based on the assumption that for inner shells screening effects come mainly from a change in normalization, as compared to the Coulomb case, and from the shift in energy corresponding to (48), as was described in more detail in Ref. 1, gives quite good results in the $1s$ case. In general, it can be expected to be correct for inner shells, where distances small on the atomic scale dominate the integration, since then the screening effects beyond normalization can be treated perturbatively.¹⁵ Denoting by $n_l (=N_l/N_l^c)$ the ratio of the screened to Coulomb normalization at the physical (not shifted) energy E , and using⁹

$$\frac{Q_2^{1c}}{D_1^{1c}} = \frac{(5)2^7}{(Z\alpha)^2} \frac{v_c^2}{(v_c^2 + 4)^2} \quad (49)$$

where $v_c = Z\alpha/p_c$, $p_c = (2E_c)^{1/2}$, and c denotes Coulomb, we obtain

$$\kappa(2s) \approx k \frac{n_2}{n_1} \frac{N_2^c}{N_1^c} \frac{(5)2^7}{(Z\alpha)^2} \frac{v_c^2}{(v_c^2 + 4)^2} \cos(\delta_2 - \delta_1) \quad (50)$$

From (48) we have $k = \frac{1}{8}(Z\alpha)^2(v_c^2 + 4)/v_c^2$, and the ratio of the Coulomb normalizations N_2^c/N_1^c is given by

$$\frac{N_2^c}{N_1^c} = \frac{P}{10} (v^2 + 4)^{1/2} \quad (51)$$

where p is the electron momentum and $v = Z\alpha/p$. For the retardation correction we get

$$\kappa(2s) \approx 8 \frac{v}{c} \frac{n_2}{n_1} \frac{(v^2 + 4)^{1/2}}{v_c^2 + 4} \cos(\delta_2 - \delta_1) \quad (52)$$

where v is the electron velocity. The corresponding expression in the ($1s$) case reads¹

$$\kappa(1s) = 2 \frac{v}{c} \frac{n_2}{n_1} (v^2 + 4)^{1/2} \cos(\delta_2 - \delta_1) \quad (53)$$

It follows from (53) that the sign of $\kappa(1s)$ is the same as the sign of $\cos(\delta_2 - \delta_1)$. Expressing $v_c^2 + 4$ as¹⁶

$$v_c^2 + 4 = \frac{4\omega}{\omega - \frac{1}{8}(Z\alpha)^2} \quad (54)$$

we see that $v_c^2 + 4 < 0$ for $\omega < \frac{1}{8}(Z\alpha)^2$, i.e., below the point-Coulomb threshold energy for the $2p$ subshell. Therefore, for final electron energies below $\frac{1}{8}(Z\alpha)^2 - \epsilon_B$, where ϵ_B is the screened binding energy of the $2p$ state, the sign of the right-hand side of (52) will be opposite to that of $\cos(\delta_2 - \delta_1)$. We may deduce in this way the sign of $\kappa(2s)$ at threshold. We may expect (52) to be a good approximation for higher energies since the semianalytic method of dealing with screening effects is better at higher energies.¹⁵ The comparison between semianalytic and numerical results in the $2s$ case is shown in Table II. The agreement between the two types of results, though in general quite good, especially for higher electron energies, is now worse than in the $1s$ case.¹ This is due to the fact that for L -shell photoelectrons, larger distances play a more important role than in the K -shell case. The agreement improves with increasing Z , since then the perturbative treatment of screening effects gives better results.¹⁵

B. The $2p$ case

Retardation corrections to the dipole angular distribution of photoelectrons ejected from the $2p$ subshell are determined by the coefficients a and b in formula (33). According to (34) and (31) they can be written as

$$a = k \frac{1}{1 + 2(D_2/D_0)^2} \left[\frac{3}{5} \frac{Q_1}{D_0} \cos\Delta_{10} - \frac{3}{5} \frac{D_2}{D_0} \frac{Q_1}{D_0} \cos\Delta_{21} - \frac{2}{5} \frac{Q_3}{D_0} \cos\Delta_{30} + \frac{7}{5} \frac{D_2}{D_0} \frac{Q_3}{D_0} \cos\Delta_{32} \right] \quad (55a)$$

$$b = k \frac{1}{1 + 2(D_2/D_0)^2} \left[\frac{8}{5} \frac{D_2}{D_0} \frac{Q_3}{D_0} \cos\Delta_{32} - 2 \frac{Q_3}{D_0} \cos\Delta_{30} - \frac{12}{5} \frac{D_2}{D_0} \frac{Q_1}{D_0} \cos\Delta_{21} \right] \quad (55b)$$

where $\Delta_{ll'} = \delta_l - \delta_{l'}$, and the dipole and quadrupole matrix elements are given by (25) and (27). Many more radial matrix elements and phase shifts are required to deter-

TABLE II. Numerical and semianalytic values of the retardation correction in the $2s$ case. The semianalytic values have been calculated according to Eq. (52) with n_2 , n_1 , δ_2 , and δ_1 calculated numerically.

E (keV)	$Z=10$		$Z=36$	
	κ (num)	κ [Eq. (52)]	κ (num)	κ [Eq. (52)]
10^{-4}	3.96×10^2	2.12×10^{-2}	-2.94×10^{-1}	-2.51×10^{-1}
10^{-3}	5.28×10^{-2}	2.96×10^{-2}	-2.10×10^{-1}	-2.10×10^{-1}
5×10^{-3}	6.65×10^{-2}	4.43×10^{-2}	8.77×10^{-2}	9.34×10^{-2}
10^{-2}	6.82×10^{-2}	5.28×10^{-2}	2.88×10^{-1}	2.98×10^{-1}
5×10^{-2}	2.60×10^{-2}	3.12×10^{-2}	3.37×10^{-1}	3.45×10^{-1}
10^{-1}	-6.97×10^{-3}	-1.01×10^{-2}	2.93×10^{-1}	2.99×10^{-1}
2×10^{-1}	-6.63×10^{-3}	-1.74×10^{-2}	2.12×10^{-1}	2.15×10^{-1}
5×10^{-1}	5.34×10^{-2}	4.45×10^{-2}	7.46×10^{-2}	7.43×10^{-2}
1.0	1.40×10^{-1}	1.36×10^{-1}	-7.20×10^{-3}	-1.04×10^{-2}
2.0	2.63×10^{-1}	2.62×10^{-1}	-1.69×10^{-2}	-2.04×10^{-2}
3.0	3.52×10^{-1}	3.54×10^{-1}	2.77×10^{-2}	2.59×10^{-2}
5.0	5.02×10^{-1}	4.94×10^{-1}	1.44×10^{-1}	1.45×10^{-1}

mine a and b than in the s -subshell case, where to determine the retardation correction κ it was necessary to know just one matrix element ratio Q_2/D_1 and one phase-shift difference $\delta_2 - \delta_1$. We therefore have not prepared a simple discussion, e.g., of the sign of a and b at threshold, of the type presented in the previous subsection.

But, despite the much greater complexity of expressions (55) as compared to the relatively simple formula (46) in the s -subshell case, the behavior of a and b as functions of photoelectron energy is numerically quite similar to the behavior of $\kappa(1s)$. In Fig. 4 we show the a - and b -retardation corrections for $Z=6$ as functions of photoelectron energy, together with the point-Coulomb results given for comparison. The coefficient a for $Z=6$ is posi-

tive, whereas b is negative at threshold and goes through zero once. Both the shape and magnitude of a and b and κ in the $1s$ case (Fig. 3) are similar. The plots of a and b for $Z=10$ (Fig. 5) look similar to those of $Z=6$, with a always positive and b negative at threshold and going through zero once. This situation changes with increasing Z . For $Z=18$ (Fig. 6), both a and b have two zeros and there is a minimum at energies close to 0.1 keV. This minimum becomes deeper with increasing Z (cf., Fig. 7 for $Z=26$ and Fig. 8 for $Z=36$), though it is, in general, less deep than in the $1s$ case. Also the magnitudes of the retardation corrections are now in general smaller than in the $1s$ case, especially at threshold. The corrections a and b are small at threshold also for these values of Z for which the $\kappa(1s)$ or $\kappa(2s)$ corrections are relatively large.

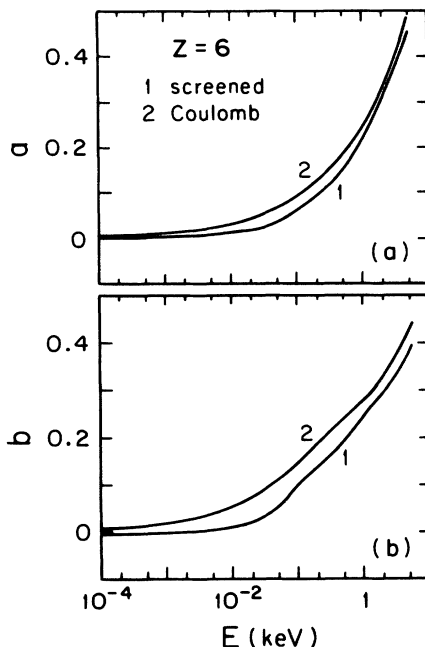


FIG. 4. Retardation corrections a and b [Eq. (55)] to the $2p$ photoelectron angular distribution, for $Z=6$.

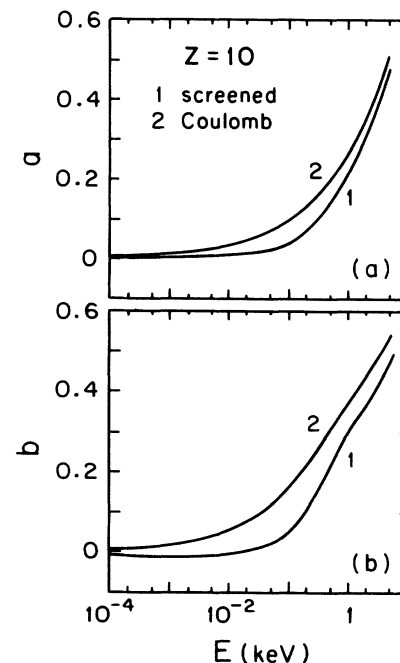
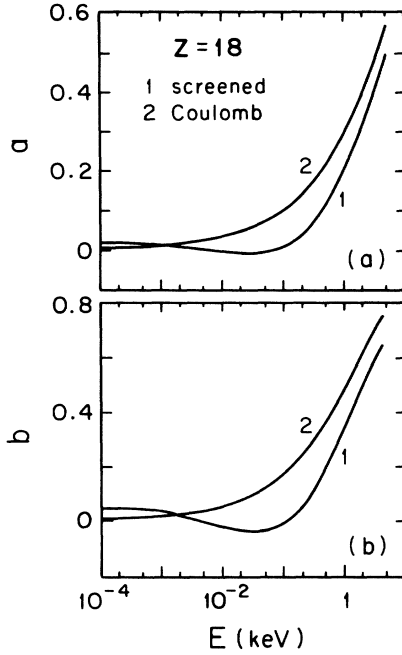
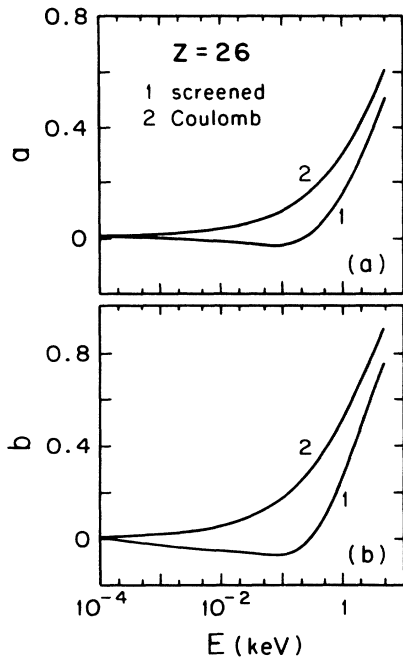
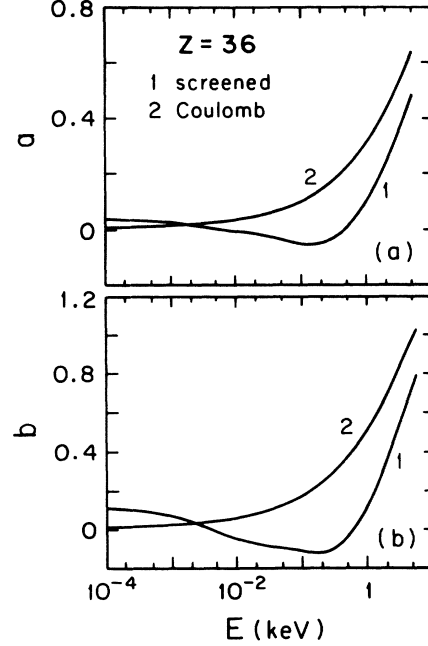


FIG. 5. Same as Fig. 4, for $Z=10$.

FIG. 6. Same as Fig. 4, for $Z=18$.

This is due to the large denominator $1+2(D_2/D_0)$ in Eq. (55), which is composed of the dipole radial matrix elements D_2 and D_0 , and, as the numerical calculation shows, $D_2 > D_0$ at threshold. This denominator is of order of 10 (e.g., ≈ 12 for $Z=6$ and ≈ 20 for $Z=36$) and therefore a and b are an order of magnitude smaller than $k(Q_1/D_1)$, which are of the same order of magnitude in the $1s$, $2s$, and $2p$ cases. As can be seen from (46), the s -subshell retardation corrections can be expected to be of the order of $k(Q_2/D_1)$, except at those energies for

FIG. 7. Same as Fig. 4, for $Z=26$.FIG. 8. Same as Fig. 4, for $Z=36$.

which $\cos(\delta_2 - \delta_1)$ is small.

Again in the $2p$ case, we have performed a semianalytic calculation similar to that described in Ref. 1 and in the previous subsection. The ratio of large-wavelength quadrupole-to-dipole matrix elements are now given by

$$k \frac{Q_3}{D_0} \approx 8Z\alpha \frac{n_3}{n_0} \frac{[(v^2+1)(v^2+4)(v^2+9)]^{1/2}}{v^3} \frac{v_c^2}{v_c^2+4}, \quad (56a)$$

$$k \frac{Q_1}{D_0} \approx -2Z\alpha \frac{n_1}{n_0} \frac{(v^2+1)^{1/2}}{v}, \quad (56b)$$

$$\frac{D_2}{D_0} \approx 4 \frac{n_2}{n_0} \frac{[(v^2+1)(v^2+4)]^{1/2}}{v^2} \frac{v_c^2}{v_c^2+4}, \quad (56c)$$

where n_1/n_0 , v , and v_c have the same meaning as in the previous subsection. Table III contains comparisons of the numerical and semianalytic results for the retardation corrections a and b as well as for the asymmetry parameter β . The agreement between both types of calculations improves with increasing energy and increasing atomic number, and is in general better for the asymmetry parameter β than for the retardation corrections a and b . The reason is that the highest angular momentum of the final state in the expressions for a and b is higher than for β (3 for a and b , 2 for β). Therefore, large distances play a more important role in the integrals determining the retardation corrections than in the case of the asymmetry parameter, and this results in a deterioration of the accuracy of the semianalytic approach for a and b as compared to β . For a similar reason, the agreement between both types of results is in general worse in the $2p$ case than for s subshells, especially when compared with the very good agreement in the $1s$ case.¹ Though in the present $2p$ case the semianalytic approach is significantly

worse than in the 1s and 2s cases, it can still be used to estimate general tendencies in the behavior of the retardation corrections as functions of energy. We note, for instance, that the semianalytical approach predicts correctly the number of zeros of a and b , though the magnitudes and signs close to the energy at which zero occurs may not agree with the numerical values. The semianalytical approach can also be used to predict whether a , b , and β are increasing or decreasing functions of energy.

To determine how large the influence of retardation corrections on the angular distribution of photoelectrons ejected from the $2p$ subshell by linearly polarized photons is, we examine the differential cross section (37) for the momentum \mathbf{p} of the final electrons perpendicular to the photon polarization vector, so that $\theta=0$ [Fig. 1(a)]. In the dipole approximation, the angular distribution in this case does not depend on the angle Φ , and

$$\left. \left(\frac{d\sigma}{d\Omega} \right) \right|_{\text{dipole}} \sim 1 - \frac{1}{2}\beta. \quad (57)$$

Including the retardation effects leads to the Φ -dependent angular distribution

$$\frac{d\sigma}{d\Omega} \sim 1 - \frac{1}{2}\beta + (a - \frac{1}{2}b)\cos\Phi. \quad (58)$$

In Table IV we show the values of $1 - \frac{1}{2}\beta$ and $a - \frac{1}{2}b$ for $Z=6, 10, 18$, and 36 , and energies ranging from 0.01 to 3 keV. At low energies (basically below 0.5 keV), the retardation effects do not contribute more than 10% to the constant dipole angular distribution, and for energies below 50 eV this contribution is of the order of $1-2\%$. The contribution of the retardation effects becomes more significant at energies of the order of 1 keV, where it can

TABLE III. Comparison between numerical and semianalytic results for the $2p$ retardation corrections a and b [Eqs. (55) and (56)] and for the asymmetry parameter β [Eqs. (32) and (56)]. Numerical and semianalytic results are given in column 1 and column 2, respectively.

E (keV)	a		b		β	
	1	2	1	2	1	2
$Z=6$						
0.0001	-1.87×10^{-4}	-3.39×10^{-3}	-6.37×10^{-3}	-2.59×10^{-2}	1.99	3.21×10^{-1}
0.001	1.98×10^{-3}	-4.09×10^{-4}	-4.72×10^{-3}	-2.17×10^{-2}	4.75×10^{-1}	5.49×10^{-1}
0.005	6.82×10^{-3}	6.73×10^{-3}	3.29×10^{-3}	-5.39×10^{-3}	1.00	1.01
0.01	1.05×10^{-2}	1.21×10^{-2}	1.03×10^{-2}	7.36×10^{-3}	1.25	1.24
0.05	3.42×10^{-2}	4.02×10^{-2}	5.43×10^{-2}	6.57×10^{-2}	1.52	1.50
0.1	6.19×10^{-2}	6.78×10^{-2}	1.02×10^{-1}	1.13×10^{-1}	1.41	1.38
0.5	1.48×10^{-1}	1.59×10^{-1}	1.95×10^{-1}	2.19×10^{-1}	6.85×10^{-1}	7.05×10^{-1}
1.0	2.15×10^{-1}	2.21×10^{-1}	2.49×10^{-1}	2.63×10^{-1}	4.22×10^{-1}	4.32×10^{-1}
2.0	3.03×10^{-1}	3.08×10^{-1}	3.04×10^{-1}	3.18×10^{-1}	1.76×10^{-1}	2.45×10^{-1}
3.0	3.65×10^{-1}	3.74×10^{-1}	3.44×10^{-1}	3.63×10^{-1}	8.00×10^{-2}	1.73×10^{-1}
5.0	4.89×10^{-1}	4.81×10^{-1}	4.52×10^{-1}	4.38×10^{-1}	-4.58×10^{-2}	1.15×10^{-1}
$Z=18$						
0.0001	1.60×10^{-2}	2.79×10^{-3}	4.61×10^{-2}	8.40×10^{-3}	1.63	1.57
0.001	1.13×10^{-2}	1.94×10^{-2}	3.33×10^{-2}	5.60×10^{-2}	1.30	1.27
0.005	3.05×10^{-4}	1.59×10^{-4}	-2.99×10^{-3}	-5.75×10^{-3}	7.14×10^{-1}	7.52×10^{-1}
0.01	-4.70×10^{-3}	-8.19×10^{-3}	-2.09×10^{-2}	-3.67×10^{-2}	5.86×10^{-1}	6.39×10^{-1}
0.05	-6.95×10^{-3}	-1.12×10^{-2}	-3.37×10^{-2}	-5.32×10^{-2}	9.88×10^{-1}	9.92×10^{-1}
0.1	6.61×10^{-3}	5.50×10^{-3}	-1.12×10^{-2}	-2.12×10^{-2}	1.26	1.24
0.5	1.11×10^{-1}	1.22×10^{-1}	1.78×10^{-1}	1.97×10^{-1}	1.46	1.45
1.0	1.97×10^{-1}	2.11×10^{-1}	3.20×10^{-1}	3.51×10^{-1}	1.32	1.33
2.0	3.07×10^{-1}	3.25×10^{-1}	4.72×10^{-1}	5.13×10^{-1}	1.04	1.09
5.0	4.93×10^{-1}	5.15×10^{-1}	6.43×10^{-1}	7.03×10^{-1}	5.54	6.90
$Z=36$						
0.0001	3.39×10^{-2}	4.59×10^{-2}	1.02×10^{-1}	1.40×10^{-1}	1.48	1.45
0.001	2.22×10^{-2}	2.43×10^{-2}	6.48×10^{-2}	2.10×10^{-1}	1.18	7.17×10^{-1}
0.005	-8.98×10^{-4}	-1.96×10^{-3}	-1.56×10^{-2}	-2.35×10^{-2}	7.06×10^{-1}	7.25×10^{-1}
0.01	-1.05×10^{-2}	-1.51×10^{-2}	-5.31×10^{-2}	-7.45×10^{-2}	5.77×10^{-1}	6.06×10^{-1}
0.05	-3.68×10^{-2}	-4.51×10^{-2}	-1.00×10^{-1}	-1.32×10^{-1}	7.57×10^{-1}	7.72×10^{-1}
0.1	-5.46×10^{-2}	-6.31×10^{-2}	-1.20×10^{-1}	-1.49×10^{-1}	9.64×10^{-1}	9.63×10^{-1}
0.5	1.13×10^{-3}	1.65×10^{-3}	-3.71×10^{-2}	-4.29×10^{-2}	1.38	1.35
1.0	9.29×10^{-2}	9.94×10^{-2}	1.29×10^{-1}	1.40×10^{-1}	1.46	1.44
2.0	2.13×10^{-1}	2.46×10^{-1}	3.77×10^{-1}	4.05×10^{-1}	1.43	1.43
3.0	3.34×10^{-1}	3.53×10^{-1}	5.51×10^{-1}	5.91×10^{-1}	1.35	1.38
5.0	4.82×10^{-1}	5.08×10^{-1}	7.81×10^{-1}	8.41×10^{-1}	1.17	1.26

TABLE IV. Parameters characterizing angular distribution of $2p$ photoelectrons in the plane perpendicular to the direction of the photon linear polarization [Eqs. (57) and (58)].

E	$Z = 6$		$Z = 10$		$Z = 18$		$Z = 36$	
	$1 - \frac{1}{2}\beta$	$a - \frac{1}{2}b$	$1 - \frac{1}{2}\beta$	$a - \frac{1}{2}b$	$1 - \frac{1}{2}\beta$	$a - \frac{1}{2}b$	$1 - \frac{1}{2}\beta$	$a - \frac{1}{2}b$
0.01	3.75×10^{-1}	5.35×10^{-3}	7.24×10^{-1}	8.88×10^{-3}	7.07×10^{-1}	5.75×10^{-3}	7.12×10^{-1}	1.61×10^{-2}
0.05	2.40×10^{-1}	7.05×10^{-3}	3.35×10^{-1}	9.00×10^{-3}	5.06×10^{-1}	9.90×10^{-3}	6.22×10^{-1}	1.32×10^{-2}
0.1	2.95×10^{-1}	1.10×10^{-2}	2.60×10^{-1}	1.06×10^{-2}	3.70×10^{-1}	1.22×10^{-2}	5.18×10^{-1}	5.40×10^{-3}
0.2	4.40×10^{-1}	2.15×10^{-2}	2.70×10^{-1}	1.51×10^{-2}	2.85×10^{-1}	1.52×10^{-2}	4.20×10^{-1}	5.90×10^{-3}
0.5	6.57×10^{-1}	5.05×10^{-2}	4.10×10^{-1}	3.15×10^{-2}	2.70×10^{-1}	2.20×10^{-2}	3.10×10^{-1}	1.79×10^{-2}
1.0	7.87×10^{-1}	8.95×10^{-2}	5.75×10^{-1}	6.20×10^{-2}	3.40×10^{-1}	3.70×10^{-2}	2.70×10^{-1}	2.84×10^{-2}
3.0	9.72×10^{-1}	1.97×10^{-1}	8.24×10^{-1}	1.60×10^{-1}	5.82×10^{-1}	1.06×10^{-1}	3.25×10^{-1}	5.85×10^{-2}

exceed 10%. This can be contrasted with the s -subshell photoeffect, where, in some cases, the retardation effects may contribute as much as 20% to the angular distribution even close to threshold. Plots of the angular distribution at $\theta=90^\circ$ for a few values of Z and energy are shown in Fig. 9.

IV. FINAL REMARKS

We have investigated in this paper higher retardation and multipole corrections to the angular distributions of photoelectrons ejected by polarized photons from the L shell. In the case of the $2s$ subshell (and in general for ns

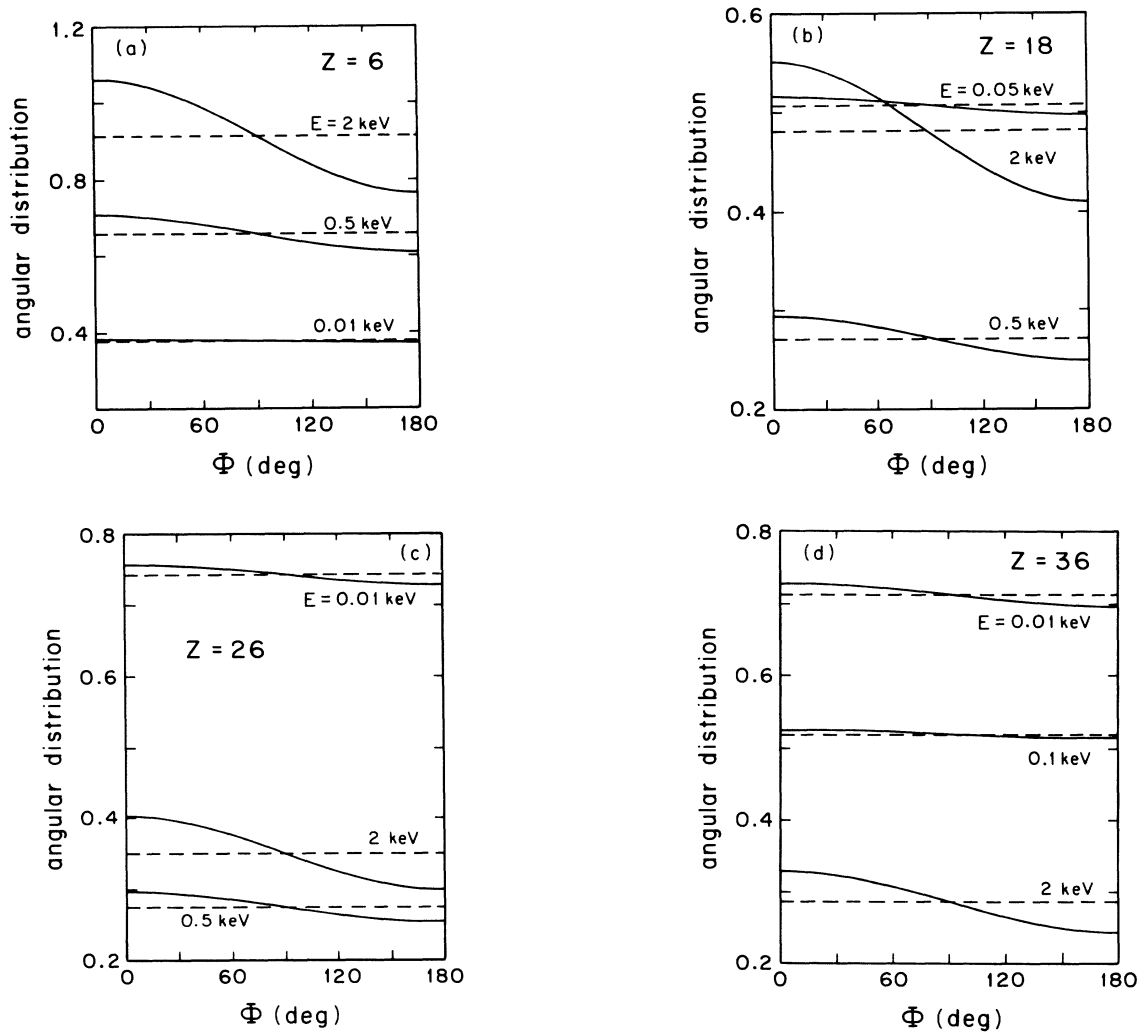


FIG. 9. Angular distribution of $2p$ photoelectrons in the plane perpendicular to the linear photon polarization. The quantity plotted is $(4\pi/\sigma)(d\sigma/d\Omega)$, with the dashed line representing the constant dipole result [Eq. (57)] and the solid line representing the angular distribution with retardation [Eq. (58)].

subshells), the retardation effects beyond the electric-dipole approximation are described by one energy-dependent parameter κ [Eq. (46)], which, even at low photoelectron energies, can be as large as 0.2–0.3, especially for higher values of the atomic number Z . For linearly polarized photons, a nonrelativistic calculation predicts vanishing s -subshell angular distribution when the electron momentum is perpendicular to the polarization vector of the photon [cf. Eq. (45)]. This result is in agreement with a recent fully relativistic calculation of Scofield,¹⁷ who obtained a very small ($\sim 10^{-3}$) relative differential cross section for 2.57 keV ($v/c=0.1$) electrons ejected from the $3s_{1/2}$ subshell of sodiumlike barium. Even at energies as high as 40–50 keV ($v/c \approx 0.4$), the relativistic relative cross section is of the order of 10^{-2} .

The leading-order retardation effects beyond the nonrelativistic dipole approximation in the $2p$ case can be described by two parameters a and b [Eqs. (33) and (35)] or B_1 and B_3 [Eqs. (35) and (36)]. The retardation effects in general are now small close to threshold and can contribute as much as 10–20% to the angular distribution at relatively low final electron energies of 1–3 keV (cf. also Ref. 13).

The retardation effects described theoretically in this paper can be observed experimentally as forward or backward peaking (depending on the sign of κ) of the angular distribution in the $2s$ case and, in the $2p$ case, as deviations from constant nonrelativistic dipole predictions for the angular distribution in the plane perpendicular to the linear photon polarization vector.

ACKNOWLEDGMENTS

The work of the first author (A.B.) was supported in part by the Polish Ministry of National Education under project No. C.P.B.P. 01-03. The work was also supported under National Science Foundation Grant No. PHY-87-04088. We wish to acknowledge helpful discussions with J. W. Cooper on his related work.

APPENDIX

This Appendix contains details of a calculation leading to formulas (24) and (26) for the transition matrix elements and to formula (30) for the angular distribution.

There are two contributions, $l=0$ and $l=2$, to the large-wavelength limit of the dipole matrix element:

$$\begin{aligned} \langle f | \boldsymbol{\epsilon} \cdot \mathbf{r} | i \rangle &= e^{i\delta_0} D_0 \int d\Omega_{\hat{\mathbf{r}}} \boldsymbol{\epsilon} \cdot \hat{\mathbf{r}} Y_{1m}(\hat{\mathbf{r}}) \\ &\quad - 5e^{i\delta_2} D_2 \int d\Omega_{\hat{\mathbf{r}}} P_2(\hat{\mathbf{p}} \cdot \hat{\mathbf{r}}) \boldsymbol{\epsilon} \cdot \hat{\mathbf{r}} Y_{1m}(\hat{\mathbf{r}}), \end{aligned} \quad (\text{A1})$$

where D_0 and D_2 are the dipole radial matrix elements (25). There are two types of angular integrals that we need to calculate:

$$\begin{aligned} I_a &= \int d\Omega_{\hat{\mathbf{r}}} \hat{x}_a Y_{1m}(\hat{\mathbf{r}}), \\ J_a &= \int d\Omega_{\hat{\mathbf{r}}} P_2(\hat{\mathbf{p}} \cdot \hat{\mathbf{r}}) \hat{x}_a Y_{1m}(\hat{\mathbf{r}}), \end{aligned} \quad (\text{A2})$$

where \hat{x}_a denotes the a th component of the unit vector $\hat{\mathbf{r}}$ (i.e., $\hat{x}_a = x_a/r$). To perform this integration effectively

we note that $Y_{1m}(\hat{\mathbf{r}})$ is a homogeneous polynomial of order 1 in the \hat{x}_a , and can therefore be written as

$$Y_{1m}(\hat{\mathbf{r}}) = \sum_b \alpha_b^{(m)} \hat{x}_b. \quad (\text{A3})$$

Thus

$$\begin{aligned} I_a &= \sum_b \alpha_b^{(m)} \int d\Omega_{\hat{\mathbf{r}}} \hat{x}_a \hat{x}_b, \\ J_a &= \sum_b \alpha_b^{(m)} \int d\Omega_{\hat{\mathbf{r}}} P_2(\hat{\mathbf{p}} \cdot \hat{\mathbf{r}}) \hat{x}_a \hat{x}_b. \end{aligned} \quad (\text{A4})$$

Using

$$\int d\Omega_{\hat{\mathbf{r}}} \hat{x}_a \hat{x}_b = \frac{4\pi}{3} \delta_{ab} \quad (\text{A5})$$

we obtain

$$I_a = \frac{4\pi}{3} \alpha_a^{(m)}. \quad (\text{A6})$$

To calculate J_a , we note that the angular integral is a symmetric tensor of rank 2, and, with two terms of this type available, i.e., δ_{ab} and $\hat{p}_a \hat{p}_b$, is of the form

$$\int d\Omega_{\hat{\mathbf{r}}} P_2(\hat{\mathbf{p}} \cdot \hat{\mathbf{r}}) \hat{x}_a \hat{x}_b = A \delta_{ab} + B \hat{p}_a \hat{p}_b. \quad (\text{A7})$$

To find A and B , we contract with respect to indices a, b which leads to

$$3A + B = \int d\Omega_{\hat{\mathbf{r}}} P_2(\hat{\mathbf{p}} \cdot \hat{\mathbf{r}}) = 0, \quad (\text{A8})$$

and multiply both sides of (A7) by $\hat{p}_a \hat{p}_b$ and sum over a and b , which gives

$$\int d\Omega_{\hat{\mathbf{r}}} P_2(\hat{\mathbf{p}} \cdot \hat{\mathbf{r}}) (\hat{\mathbf{p}} \cdot \hat{\mathbf{r}})^2 = A + B. \quad (\text{A9})$$

Expressing $(\hat{\mathbf{p}} \cdot \hat{\mathbf{r}})^2$ as a combination of P_2 and P_0 and using the orthogonality relations for the Legendre polynomials, we get

$$A + B = \frac{8\pi}{15}. \quad (\text{A10})$$

From (A8) and (A10) we have $A = -4\pi/15$, $B = 4\pi/5$, so that

$$\int d\Omega_{\hat{\mathbf{r}}} P_2(\hat{\mathbf{p}} \cdot \hat{\mathbf{r}}) \hat{x}_a \hat{x}_b = -\frac{4\pi}{15} (\delta_{ab} - 3\hat{p}_a \hat{p}_b) \quad (\text{A11})$$

and

$$J_a = -\frac{4\pi}{15} [\alpha_a^{(m)} - 3\hat{p}_a Y_{1m}(\hat{\mathbf{p}})]. \quad (\text{A12})$$

For the matrix element (A1) we have

$$\begin{aligned} \langle f | \boldsymbol{\epsilon} \cdot \mathbf{r} | i \rangle &= \frac{4\pi}{3} \{ e^{i\delta_0} D_0 Y_{1m}(\boldsymbol{\epsilon}) \\ &\quad + e^{i\delta_2} D_2 [Y_{1m}(\boldsymbol{\epsilon}) - 3\boldsymbol{\epsilon} \cdot \hat{\mathbf{p}} Y_{1m}(\hat{\mathbf{p}})] \}, \end{aligned} \quad (\text{A13})$$

which is the same as (24). In passing from (A11) to (A12), as well as to (A13), we used (A3) with $\hat{\mathbf{r}}$ replaced either by $\boldsymbol{\epsilon}$ or $\hat{\mathbf{p}}$.

To calculate the electric quadrupole matrix element (26), we note first that for the p initial state there are only $l=1$ and $l=3$ contributions. We have, therefore,

$$\langle f | (\hat{\mathbf{k}} \cdot \mathbf{r})(\boldsymbol{\epsilon} \cdot \mathbf{r}) | i \rangle = 3i^{-1} e^{i\delta_1} Q_1 \int d\Omega_{\hat{\mathbf{r}}} P_l(\hat{\mathbf{p}} \cdot \hat{\mathbf{r}})(\hat{\mathbf{k}} \cdot \hat{\mathbf{r}})(\boldsymbol{\epsilon} \cdot \hat{\mathbf{r}}) Y_{1m}(\hat{\mathbf{r}}) - 7i^{-1} e^{i\delta_3} Q_3 \int d\Omega_{\hat{\mathbf{r}}} P_3(\hat{\mathbf{p}} \cdot \hat{\mathbf{r}})(\hat{\mathbf{k}} \cdot \hat{\mathbf{r}})(\boldsymbol{\epsilon} \cdot \hat{\mathbf{r}}) Y_{1m}(\hat{\mathbf{r}}). \quad (\text{A14})$$

The two angular integrals that have to be calculated are

$$I_{ab}^l = \int d\Omega_{\hat{\mathbf{r}}} P_l(\hat{\mathbf{p}} \cdot \hat{\mathbf{r}}) \hat{x}_a \hat{x}_b Y_{1m}(\hat{\mathbf{r}}), \quad (\text{A15})$$

with $l=1$ and $l=3$. Using (A3), we obtain

$$I_{ab}^l = \sum_c \alpha_c^{(m)} \int d\Omega_{\hat{\mathbf{r}}} P_l(\hat{\mathbf{p}} \cdot \hat{\mathbf{r}}) \hat{x}_a \hat{x}_b \hat{x}_c. \quad (\text{A16})$$

The angular integral is a totally symmetric tensor of rank 3, and must therefore be of the form

$$\int d\Omega_{\hat{\mathbf{r}}} P_l(\hat{\mathbf{p}} \cdot \hat{\mathbf{r}}) \hat{x}_a \hat{x}_b \hat{x}_c = A (\delta_{ab} \hat{p}_c + \delta_{ac} \hat{p}_b + \delta_{bc} \hat{p}_a) + B \hat{p}_a \hat{p}_b \hat{p}_c. \quad (\text{A17})$$

The equations determining A and B are

$$\begin{aligned} 5A + B &= \int d\Omega_{\hat{\mathbf{r}}} P_l(\hat{\mathbf{p}} \cdot \hat{\mathbf{r}})(\hat{\mathbf{p}} \cdot \hat{\mathbf{r}}), \\ 3A + B &= \int d\Omega_{\hat{\mathbf{r}}} P_l(\hat{\mathbf{p}} \cdot \hat{\mathbf{r}})(\hat{\mathbf{p}} \cdot \hat{\mathbf{r}})^3. \end{aligned} \quad (\text{A18})$$

Using $x = P_1(x)$, $x^3 = \frac{2}{5}P_3(x) + \frac{3}{5}P_1(x)$, we obtain

$$\begin{aligned} \langle f | (\hat{\mathbf{k}} \cdot \hat{\mathbf{r}})(\boldsymbol{\epsilon} \cdot \hat{\mathbf{r}}) | i \rangle &= -\frac{4\pi}{5} i e^{i\delta_1} Q_1 [(\boldsymbol{\epsilon} \cdot \hat{\mathbf{p}}) Y_{1m}(\hat{\mathbf{k}}) + (\hat{\mathbf{p}} \cdot \hat{\mathbf{k}}) Y_{1m}(\boldsymbol{\epsilon})] \\ &+ \frac{4\pi}{5} i e^{i\delta_3} Q_3 [-(\boldsymbol{\epsilon} \cdot \hat{\mathbf{p}}) Y_{1m}(\hat{\mathbf{k}}) - (\hat{\mathbf{p}} \cdot \hat{\mathbf{k}}) Y_{1m}(\boldsymbol{\epsilon}) + 5(\boldsymbol{\epsilon} \cdot \hat{\mathbf{p}})(\hat{\mathbf{p}} \cdot \hat{\mathbf{k}}) Y_{1m}(\hat{\mathbf{p}})], \end{aligned} \quad (\text{A22})$$

which is the same as (26).

To find the angular distribution, we use (28) with

$$\begin{aligned} M^{\text{dipole}} &= -\omega \langle f | \boldsymbol{\epsilon} \cdot \mathbf{r} | i \rangle, \\ M^{\text{ret}} &= -\frac{1}{2} \omega k \langle f | (\hat{\mathbf{k}} \cdot \mathbf{r})(\boldsymbol{\epsilon} \cdot \mathbf{r}) | i \rangle. \end{aligned} \quad (\text{A23})$$

In performing the summation over the magnetic quantum number, we use the summation formulas (29) for spheri-

$$\begin{aligned} 5A + B &= \frac{4\pi}{3} \delta_{l1}, \\ 3A + B &= \frac{8\pi}{35} \delta_{l3} + \frac{4\pi}{5} \delta_{l1}, \end{aligned} \quad (\text{A19})$$

which gives

$$A = \frac{4\pi}{15} \delta_{l1} - \frac{4\pi}{35} \delta_{l3}, \quad B = \frac{4\pi}{7} \delta_{l3}. \quad (\text{A20})$$

Substituting (A20) into (A17) and then into (A16) yields

$$\begin{aligned} I_{ab}^1 &= \frac{4\pi}{15} [\delta_{ab} Y_{1m}(\hat{\mathbf{p}}) + \alpha_a^{(m)} \hat{p}_b + \alpha_b^{(m)} \hat{p}_a], \\ I_{ab}^3 &= -\frac{4\pi}{35} [\delta_{ab} Y_{1m}(\hat{\mathbf{p}}) + \alpha_a^{(m)} \hat{p}_b + \alpha_b^{(m)} \hat{p}_a] \\ &+ \frac{4\pi}{7} \hat{p}_a \hat{p}_b Y_{1m}(\hat{\mathbf{p}}), \end{aligned} \quad (\text{A21})$$

and, upon substituting (A21) into (A14), we obtain

cal harmonics, noting that

$$\sum_m Y_{1m}^*(\hat{\mathbf{k}}) Y_{1m}(\boldsymbol{\epsilon}) = \frac{3}{4\pi} \mathbf{k} \cdot \boldsymbol{\epsilon} = 0, \quad (\text{A24})$$

$$\sum_m Y_{1m}^*(\hat{\mathbf{n}}) Y_{1m}(\hat{\mathbf{n}}) = \frac{3}{4\pi} P_1(1) = \frac{3}{4\pi}, \quad (\text{A25})$$

where $\hat{\mathbf{n}}$ may denote any of the unit vectors $\hat{\mathbf{k}}$, $\hat{\mathbf{p}}$, or $\boldsymbol{\epsilon}$.

*Permanent address: Institute of Physics, University of Szczecin, Wielkopolske 15, 70-451 Szczecin, Poland.

¹A. Bechler and R. H. Pratt, Phys. Rev. A **39**, 1774 (1989).

²J. Cooper and R. N. Zare, in *Lectures in Theoretical Physics* (Gordon and Breach, New York, 1968), Vol. XI-C.

³R. H. Pratt, A. Ron, and H. K. Tseng, Rev. Mod. Phys. **45**, 273 (1973).

⁴K. N. Huang, Phys. Rev. A **22**, 223 (1980); **26**, 3676 (1982).

⁵This does not mean that v/c is the true expansion parameter. It is the expansion parameter in the Coulomb case, when the retardation correction vanishes at threshold (cf. Ref. 2). In the screened case, however, the retardation correction may not vanish at threshold, being of the order $Z\alpha$ rather than v/c . The retardation correction is expected not to be large if ka , where a is the size of the region contributing to the integral in the matrix element, is not large. For an inner shell with principal quantum number n , ka is equal to $[(E + \epsilon_B)/mc^2](n/Z\alpha)$, where E is the continuum electron

energy and ϵ_B is the binding energy. In the Coulomb case this quantity is $\sim Z\alpha$ at threshold—the vanishing of the Coulomb retardation correction at threshold for the K shell is due to $\cos(\delta_2 - \delta_1) \sim v/c \rightarrow 0$. In the screened case, the $\cos(\delta_2 - \delta_1)$ in general does not vanish at threshold. Note also that the retardation expansion is not an expansion in powers of k since it does not account for the k dependence of the final electron energy due to energy conservation.

⁶H. A. Bethe and E. E. Salpeter, *Quantum Mechanics of One and Two Electron Atoms* (Springer-Verlag, Berlin, 1957), p. 269.

⁷The Pauli-Schrödinger term is linear in the electron spin, and will give a contribution of the same type to the cross section if only those terms up to and including $\sim k$ are kept. Thus it does not affect the angular distribution of unpolarized final electrons but has to be taken into account, e.g., in the investigation of the full polarization correlations.

⁸One can pass directly from the velocity form of the radial ma-

trix elements (3) to the length form (6) by using the commutation relation $ip_r = [r, H]$ with the radial component of the momentum operator $p_r = i^{-1}(\partial/\partial r + r^{-1})$ (cf. also Ref. 1).

⁹M. S. Wang, unpublished.

¹⁰For a polarized beam with the polarization vector in the x - y plane (\mathbf{k} along the z axis), ξ_1, ξ_2, ξ_3 are given by

$$\xi_1 = |\epsilon_x|^2 - |\epsilon_y|^2,$$

$$\xi_2 = \epsilon_x \epsilon_y^* + \epsilon_x^* \epsilon_y,$$

$$\xi_3 = i(\epsilon_x \epsilon_y^* - \epsilon_x^* \epsilon_y).$$

¹¹I. B. Goldberg and P. M. Bergstrom, Jr. (unpublished).

¹²R. H. Pratt, R. Y. Yin, and Xiaoling Liang, Phys. Rev. A **35**, 1450 (1987).

¹³S. T. Manson, Phys. Rev. A **31**, 3698 (1985).

¹⁴A zero in the dipole transition from $2s$ to an ϵp state may, however, occur for $\epsilon < 0$ and bigger than the energy of the bound $2s$ state. The theory described in Ref. 11 predicts an odd number of zeros in D_1 in the range of energies from (negative) ϵ_{20} to ∞ .

¹⁵J. McEnnan, L. Kissel, and R. H. Pratt, Phys. Rev. A **13**, 532 (1976).

¹⁶Equation (54) follows from (48) and the energy conservation $E + \epsilon_B = \omega$, where ϵ_B is the screened binding energy.

¹⁷J. H. Scofield, Phys. Rev. A **40**, 3054 (1989).